

Title: Annealing of ion irradiation damage in nuclear graphite¹

Authors: Michael Lasithiotakis^{*2,a,b}, Barry J. Marsden^b and T. James Marrow^c.

a-Materials Performance Centre, Corrosion and Protection Centre, School of Materials,
The University of Manchester, Manchester, M13 9PL, UK

b-Nuclear Graphite Research Group. School of Mechanical, Aerospace and Civil
Engineering, The University of Manchester, Manchester M13 9PL, UK.

c- Department of Materials. University of Oxford, Parks Road, Oxford OX1 3PH, UK

¹ NOTICE: this is the author's version of a work that was accepted for publication in Journal of Nuclear Materials. Changes resulting from the publishing process, such as peer review, editing, corrections, structural formatting, and other quality control mechanisms may not be reflected in this document. Changes may have been made to this work since it was submitted for publication. A definitive version was subsequently published in Journal of Nuclear Materials **434**(1-3):334-346 2013, <http://dx.doi.org/10.1016/j.jnucmat.2012.12.001>

² ***Corresponding author:** Tel: +44(0)161 306 4840. e-mail: Michael.Lasithiotakis@postgrad.manchester.ac.uk

Abstract

Changes in Raman spectra of polished and ion-irradiated Gilsocarbon and Highly Orientated Pyrolytic Graphite (HOPG) during annealing have been investigated and compared with changes reported during stored energy release in fast neutron irradiated graphite. It is postulated that the change in the Raman spectra of polished, ion-irradiated and neutron irradiated graphite can be attributed to crystalline structural changes due to the annealing of lattice defects. This is illustrated in this work by changes in the kinetic parameters, in terms of the decrease of the Raman I_D/I_G ratio, during the thermal annealing of polished and ion-irradiated Gilsocarbon and HOPG graphite. Several kinetic models are investigated in terms of activation energy and order of reaction. The most suitable model to explain Raman annealing kinetics was found to be, a two reaction model for polished Gilsocarbon graphite, and a two and possibly three reaction model for ion-irradiated Gilsocarbon graphite and ion-irradiated HOPG. The kinetics parameters obtained using both the two and three reaction models reveal similarities with kinetic models obtained for neutron irradiated graphite. The assumption that the Raman intensity ratio I_D/I_G is proportional to the square root of the defect quantity provided a better fit than the assumption of direct proportionality.

1 Introduction

Ion irradiation is an attractive technique often used to simulate neutron irradiation, because it can allow study of irradiation damage without the need to deal with radioactive

materials. High fluence can be achieved in relatively short times, although the depth of penetration is shallow. It is also attractive as access to neutron-irradiated samples is often difficult and limited.

There is a wide range of ion irradiation techniques available. Typically ions from noble gases such as Ar, He or Xe and Kr are used [1-8]. The technique normally employs a simple ion beam, sometimes defocused [7] and sometimes in a plasma form [4]. Ions can be obtained from different noble gases directly [2] or even the same ion in different molecular states [5] in order to execute comparative studies with respect to size of the particle inducing damage. There are some examples where two different ions have been used simultaneously such as in the work of Asari et al. [1] who used He^+ as the basic irradiation ion, together with some incidental irradiation of Ar^+ . It is also possible to use other types of ions such as in the work of Liu et al. [3] who irradiated highly oriented pyrolytic graphite with heavy ions, mostly from metals (Ne, Cr, Fe, Ni, Zn, Xe and U).

The main differences between ion irradiation and neutron irradiation are: a) the larger size of the colliding particle compared to neutrons (Ar^+ ions of 39 molecular weight are very frequently used, and are gigantic compared to the molecular weight of a neutron), b) the charge (neutrons have no charge), and the lower energies applied (usually ions have energies of the range from a few keV to a few hundred keV, while neutrons reach higher energies up to ~ 10 MeV in a fission system or 14 MeV in a fusion system). Despite these differences, many researchers use ion irradiation as a primary technique for the study of irradiation damage in graphite. In this study the thermal annealing behaviour of ion-

irradiated samples is investigated using kinetic modelling and comparisons are made between neutron and ion irradiation.

The graphite grades irradiated with ions were Gilsocarbon³ and Highly Oriented Pyrolytic Graphite (HOPG). Gilsocarbon is polycrystalline artificial graphite manufactured from a spherical, onion-like coke produced from naturally occurring asphalt mined in the USA called Gilsonite. The spherical shape of this coke ensures that moulded Gilsocarbon graphite has no strong preferential alignment. This type of graphite was used as a moderator in the UK Advanced Gas Reactors [9].

HOPG is manufactured by a vapour deposition method, which produces a lamellar structure of stacked planes. When graphitised under compression HOPG⁴ is highly crystalline, consisting of layers of two-dimensional graphitic planes. HOPG is often used in ion irradiation studies [5, 7, 8]. The purpose of studying irradiation in HOPG is that HOPG is considered to be a good approximation of a graphitic single crystal, and the resulting damage in HOPG is relatively easily observable using microscopy techniques.

³ Supplied by British Energy Generation Ltd (now part of EDF Energy)

⁴ SPI Supplies. Mr. Harry Hargreaves. Aztech Trading, 12 Kernan Drive, Swingbridge Trading Estate, Loughborough Leicestershire LE11 5JF England. UK.

2 Experimental

2.1 *Sample preparation*

2.1.1 Gilsocarbon

A specimen of Gilsocarbon was embedded in a cylindrical resin mould and machined with a diamond impregnated cutting disc into small samples approximately 3 mm x 3 mm x 2 mm. Then the resin mould was cut into thin slices and from this graphite specimens (3 mm x 3 mm x less than 0.5 mm thickness) were separated manually. During cutting, water was used for cooling and lubrication; therefore the separated specimens were dried for 24 hours at room temperature.

The Gilsocarbon specimens were then manually ground using silicon carbide paper of P800 grade (21.8 μm) followed by silicon carbide paper of P4000 grade (5 μm). Then as a second stage, the samples were polished with diamond paste (Preparationes Diamantee Mecaprex) with a nominal mean grain size of 3 μm then 1 μm consecutively to further remove scratches and preparation artefacts. The purpose of polishing was: a) to prepare the surfaces for ion irradiation b) to explore the effect of the production of defects introduced on the surface of the material by polishing.

2.1.2 Highly Oriented Pyrolytic Graphite

A specimen of HOPG was similarly immersed in resin and cut into pieces of approximately 3 mm x 3 mm x 0.5 mm. Then, the resin was removed and each specimen was cleaved with adhesive tape in order to produce many specimens with less than 0.5

mm thickness. Finally, the surfaces were smoothed by a technique of successive removal of damaged surfaces layers with adhesive tape to produce a clear “mirror” surface [10]

2.2 Ion irradiation and annealing

2.2.1 Irradiation method and penetration depth

Ion irradiation was achieved using a Gatan PIPS ion beam milling device, designed to prepare specimens for transmission electron microscopy (TEM). This device uses two Argon beams directed from opposite directions. The available energy of irradiation is between 1 and 6 keV, and the angle of irradiation can be up to 10° from the sample surface. The irradiation chamber is maintained in a vacuum (10^{-4} - 10^{-7} torr) at ambient temperature. Five samples of Gilsocarbon and five of HOPG were ion-irradiated in this way, with an energy of 6keV for four hours. The angle of irradiation was maintained at 5° . The maximum achievable current intensity varied between 30-40 mA. During irradiation the beam intensity was observed to periodically vary (approximate sinusoidal variation of five seconds time period) between 4 and 30 mA. A pressure of 10^{-5} torr was maintained throughout. Samples were rotating at 6 revolutions per minute; the maximum speed available. Atomic displacements caused by the ions and subsequent cascades were calculated using the TRIM code⁵ (Transport of Ions in Matter), [11]. Penetration depths were calculated of less than 80-90 nm for HOPG and less than 120-130 nm for Gilsocarbon, which is due to the difference in density between the two graphite grades.

⁵ Transport of Ions in Matter (TRIM). Software by Ziegler JF, Ziegler MD, Biersack JP. 2008. Available at <http://www.srim.org>

The irradiation damage intensity significantly decreases from a depth of 50-60 nm for HOPG and 70-80 nm for Gilsocarbon.

2.2.2 Annealing

Annealing took place under an argon atmosphere in a tube furnace. The input gas was 99.999% pure with traces of oxygen, which were removed using activated copper. The heating program consisted of three stages: heating to the chosen temperature at a rate of approximately $10^{\circ}\text{C min}^{-1}$, then holding the furnace at temperature for at least half an hour, before cooling down to room temperature. This heating program was repeated several times, each time with a final temperature of 50°C higher than previous time. After cooling down, and before each next consecutive heating, Raman spectroscopy tests were carried out, as will be described in Section 3.3. The temperature for first heating was 100°C and for the last heating 600°C .

This heating cycle was chosen following the report of Borisov et.al [12] who annealed ion irradiating graphite samples at 35 keV followed by annealing resulting in a restoration of the initial condition after one hour. Therefore in this work, it has been assumed that an annealing time of 30 minutes for specimens bombarded with lower energy 6 keV Ar^{+} ions would ensure sufficient termination of all annealing reactions..

2.3 Raman spectroscopy

Raman spectroscopy is a useful technique for monitoring the changes of molecular states after ion-irradiation. Previous researchers have investigated the Raman spectra in a varieties of carbon materials [1, 5, 7, 8, 13] obtaining spectra in intact (virgin) graphite as

well as processed samples (polished, neutron or ion-irradiated, deposited etc). The Raman spectra proved to be very sensitive even to slight alterations to the surfaces.

The basic peaks observed in a Raman spectrum of a graphitic material [1-6, 8, 10, 13] are a first order peak at approximately 1580 cm^{-1} designated the G mode (after the space symmetry E_{2g}), and three other first-order peaks found between $1340\text{-}1346\text{ cm}^{-1}$ (D_1) and at approximately 1367 cm^{-1} (D_2) and 1622 cm^{-1} (D_0). These last three peaks are designated as D modes and are attributed to the disorder in the graphitic structures. For example, the D_1 peak at around 1340 cm^{-1} is a breathing mode of A_{1g} symmetry [14]. This mode is forbidden in perfect graphite and only becomes active in the presence of disorder. Such disorder is assumed to indicate the destruction of the sp^2 standard graphitic structure, and the production of defects that can be attributed to sp^3 hybridism. It is also assumed [15] that the production of defects results in creation of diamond like clusters, formed by sp^3 hybridism bonds. The region of second-order Raman spectra shows four distinct peaks at 2680 ($2D_1$), 2730 ($2D_2$), 3250 ($2D_0$) cm^{-1}

One of the basic Raman parameters used in tracking changes in molecular states of graphite is the relative intensity of the D_1/G peaks. For example, it has been observed [8] that this ratio increases after ion irradiation of pristine HOPG. The D_1 mode has been observed [7] to occur when the ion irradiation fluence reaches a critical value, which decreases for heavier ions. Hida et al. [8] showed how the charge state of the colliding particle affected the D_1/G ratio in HOPG. The D_1/G ratio is also reported to vary with other types of damage. For example Nakamizo et al. [15] reported that polishing a graphitic surface resulted in significant increase of the D_1/G ratio.

In this work, Raman spectroscopy is used to investigate the annealing of defects in Gilsocarbon and HOPG caused by ion irradiation and by mechanical polishing. Raman spectroscopy measurements were carried out using a Renishaw Wire 633nm UV laser source Raman spectrometer. For simplicity, the D_1 peak will be referred to as the D peak, and the D_1/G peak intensity ratio will be denoted as I_D/I_G .

The Raman spectra of polished Gilsocarbon, ion-irradiated Gilsocarbon and HOPG are compared with the spectra from non-irradiated HOPG, selected features exposed by the fracture of Gilsocarbon, and that of a neutron-irradiated nuclear graphite machined from a sample extracted from British Experimental Pile Zero, (BEPO⁶), at Harwell; this latter sample was irradiated in air to an irradiation fluence of $11.3 \times 10^{20} \text{ n cm}^{-2}$ at a temperature between 100 and 120°C. It should be noted that during operation the BEPO graphite core was annealed several times in an attempt to reduce the levels of stored energy [16]); this may have affected the irradiation damage. Raman spectra representative of some of the samples are shown in Figure 1.

⁶ Irradiated BEPO graphite was supplied by the United Kingdom Atomic Energy Authority with permission of the United Kingdom Nuclear Decommissioning Authority.

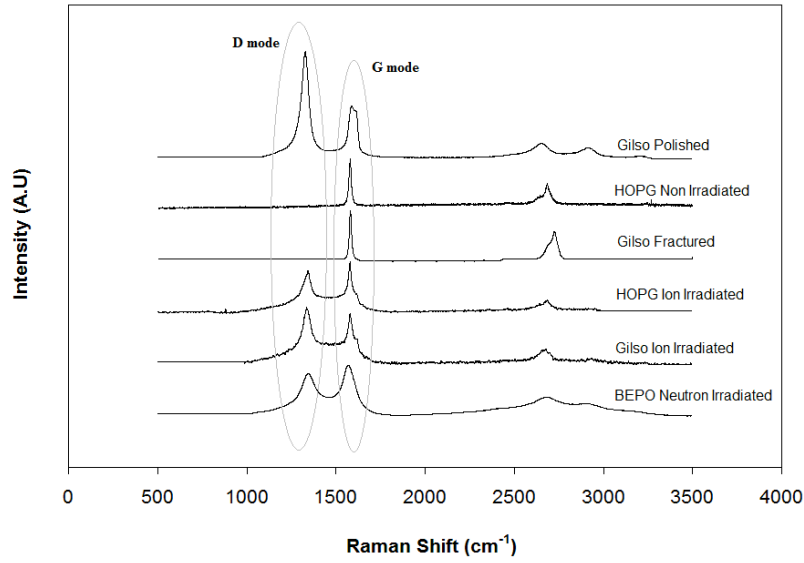


Figure 1: Raman spectra of neutron-irradiated BEPO graphite compared to ion-irradiated HOPG, ion-irradiated Gilsocarbon, and polished Gilsocarbon

In Figure 1, a comparison between BEPO neutron irradiated graphite spectra (Fig 1, bottom), and Gilsocarbon and HOPG ion irradiated graphites (Fig 1, the next two from bottom to top) shows broader features in the D and G bands of BEPO compared with Gilsocarbon and HOPG. Such broadening of the G and D peaks has also been reported in the Raman spectra obtained for a graphite block that had been exposed to the edge plasma produced in the TEXTOR tokamak (Tokamak Experiment for Technology Oriented Research) at around 300 to 400°C [17]. The formation of thermally stable defects was proposed as an explanation for this..

Optical microscopy observations on the fractured surface of Gilsocarbon reveal reflective facets that are considered to be pre-existing calcination or graphitisation cracks (Figure 2). Raman spectra were obtained from these facets. The cracks arise during manufacture

due to the large anisotropy of graphite crystallite thermal expansion, they are therefore assumed to be close to the crystal basal plane. By using fracture to expose pre-existing cracks, no deformation is introduced to the facet surface, in contrast to surface preparation by cutting or polishing.

In non-irradiated HOPG and on the facets of fractured Gilsocarbon, there is a complete absence of the D peak, see Figure 1, indicating that there are no significant disturbed zones on the structure of the surfaces of these samples. Ion-irradiated HOPG and Gilsocarbon have substantial D peaks, similar to that of neutron-irradiated graphite in terms of peak height and shape. Mechanical polishing of Gilsocarbon graphite produced a substantial D peak, almost twice the G peak intensity, since polishing produces large quantities of surface defects; as reported by previous authors in other graphite grades [15].

The peaks appearing at approximately 1500 cm^{-1} on the irradiated HOPG and Gilsocarbon specimens arise from the overlap of sharp peaks with a background broader peak. The overlapping of the broad background Raman band and sharp Raman peaks has been shown to be a typical feature for graphite irradiated with heavy ions of noble gases under low incident energy; the energy deposition on the graphite surface alters the optical skin depth extensively [18]. Niwase et al. [19] showed differences in the nature between the sharp and the broad Raman peaks and connected them with optical skin depth. They also monitored Raman spectra of ion irradiated graphite annealed below 600°C , and showed that the changes occurred for the sharp Raman peaks at a lower dose. The broad Raman band has been shown [19, 20], to be more stable, with reduction in its intensity

occurring on annealing for higher doses where amorphization due to irradiation had taken place

Specimens of ion-irradiated Gilsocarbon, ion-irradiated HOPG, and polished Gilsocarbon, were annealed to 100°C for 30 min, as previously described. After annealing and cooling to room temperature Raman measurements were repeated on the same specimens followed by another annealing cycle to 150°C. Such cycles of consecutive annealing and Raman measurement continued in steps of 50°C until a temperature of 600°C was reached.

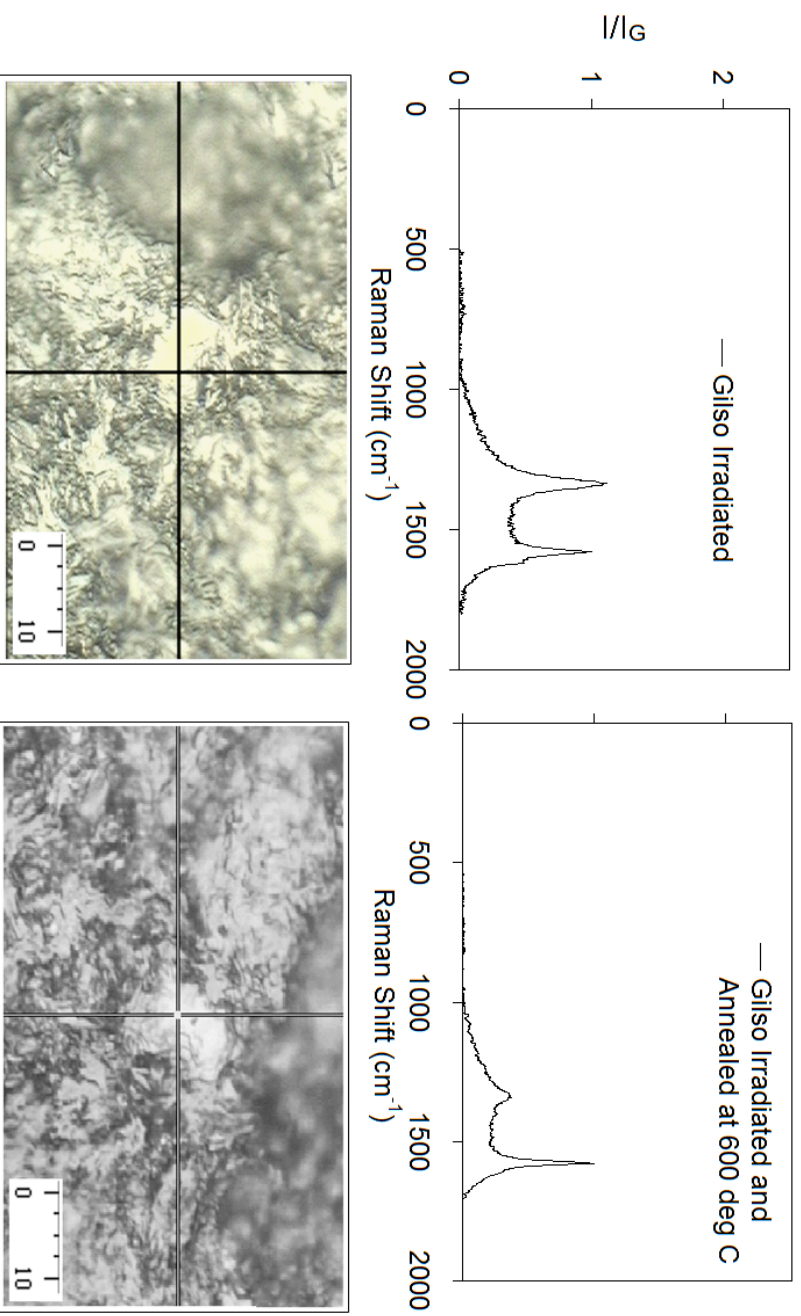


Figure 2: A comparison between two spectra of Gilso carbon irradiated with Argon ions (left) and the same specimen annealed at 600°C (right). I/I_G versus Raman shift. Below each spectrum is an optical microscopy image of the measurement area (scale in μm). A noticeable reduction in the heights of D and G peaks is observed after annealing at 600°C

Raman measurements on the same samples before annealing showed noticeable differences in the spectra with position (up to 20% variation). An optical microscopic image was therefore used to accurately locate the same position on the sample surface for each Raman measurements after each annealing cycle (Figure 2). All the measurements were taken three times to assure reproducibility. The ratio of the D and G peak (I_D/I_G) was obtained from the spectra. Reproducibility was observed to be very high, with a variation of less than 0.1%.

The Raman spectra of irradiated Gilsocarbon (Fig.2) and irradiated HOPG (Fig.4 right, bottom and top), unlike polished Gilsocarbon (Fig.4 left, bottom and top), exhibit the overlapping of sharp Raman peaks and at least one broad Raman peak. These specimens, when annealed, displayed a remarkable decrease in the sharp Raman peaks, whereas the broad Raman peak did not display any significant decrease. This is due to irradiation-induced disordering and characteristic of Raman spectrum for graphite irradiated with heavy ions of low incident energy [19].

Raman spectra at the various annealing temperatures on the ion-irradiated Gilsocarbon specimen are shown in Figure 3. All the measurements exhibit both D and G peaks and the I_D/I_G ratio was observed to decrease progressively with each annealing cycle. The same behaviour was observed for ion-irradiated HOPG and polished Gilsocarbon. A comparison between Raman spectra for ion-irradiated HOPG and polished Gilsocarbon at the end of the 600°C annealing cycle is given in Figure 4, in which the marked decrease of relative intensity of the D peak is clearly evident.

The relationship between the annealing temperature and the I_D/I_G ratio, normalised by its value before the first anneal, is given in Figure 5 for all three specimens. The

decrease in I_D/I_G is more significant for the irradiated Gilsocarbon and HOPG specimens than for the polished Gilsocarbon sample, which shows a significant drop only after annealing above 350°C. This may indicate differences in the nature of the defects produced by irradiation and polishing.

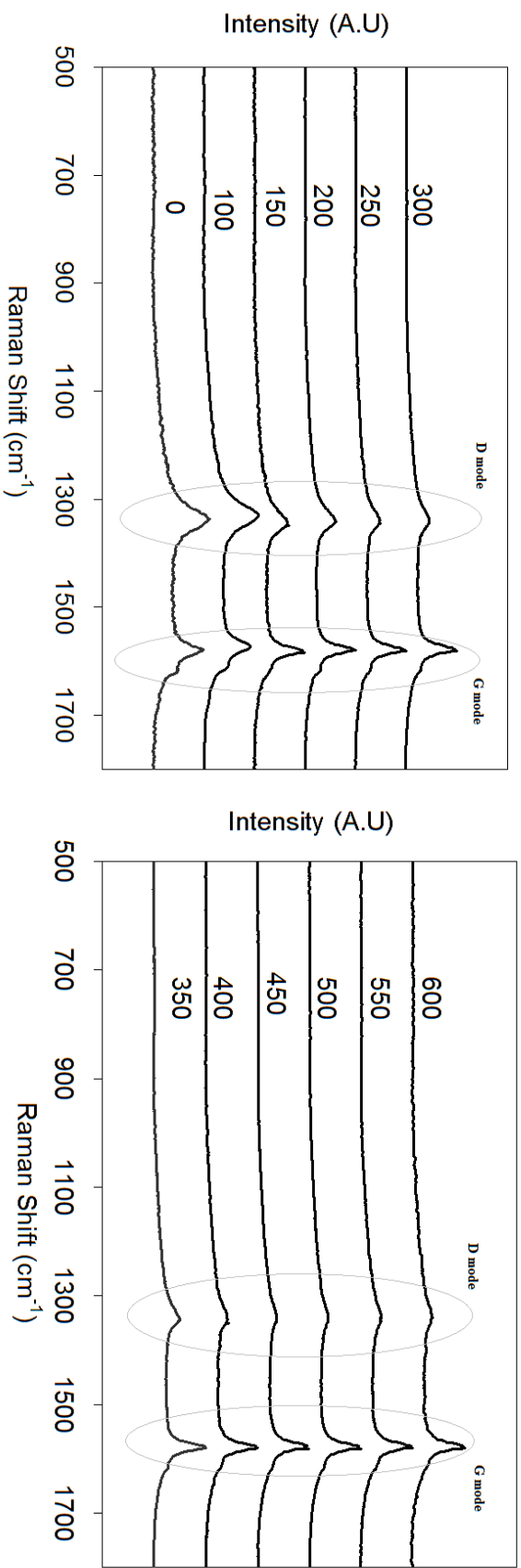


Figure 3. A collection of all Raman spectra for various annealing temperatures (°C) of the Ar⁺ ion-irradiated Gilsocarbon specimen

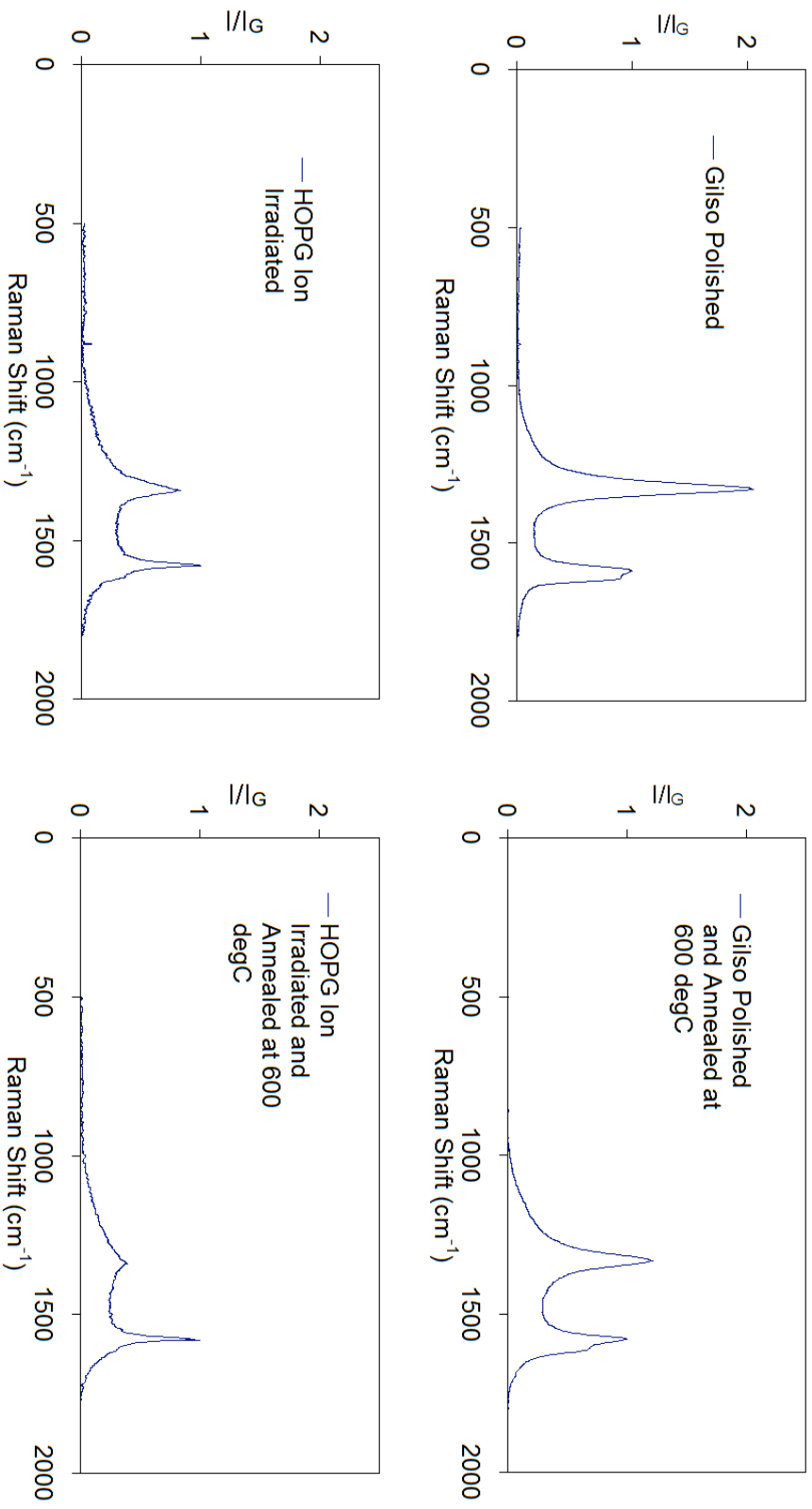


Figure 4: A comparison between two spectra of Gilso carbon polished (top), and HOPG irradiated with Argon ions (bottom) and the same specimens annealed at 600°C

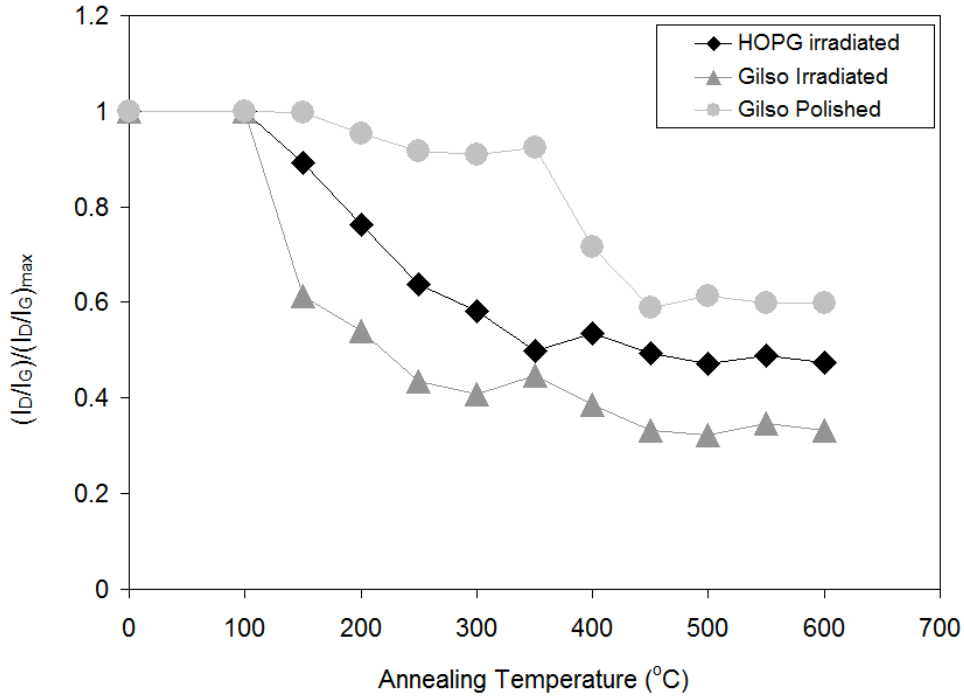


Figure 5: Annealing temperature versus I_D/I_G normalised by the initial I_D/I_G ratio for Gilsocarbon and HOPG irradiated with Argon ions and polished Gilsocarbon.

3 Analysis

The decrease in the relative intensity of the D peak is considered to be indicative of a decrease in the number of defects with thermal treatment (annealing). A general assumption is made that by calculating the I_D/I_G ratio it is possible to extract quantitative information about the population of defects present.

The quantity of defects, Q , is assumed to be directly proportional to the I_D/I_G ratio since I_G , the intensity of the G peak, is assumed to be directly associated with the $A1g$ symmetry, which is unaffected by irradiation damage [1-6, 8, 13, 14].

$$Q = \lambda \frac{I_D}{I_G} \quad (1)$$

where λ is a factor of proportionality.

3.1 Kinetic model

The process of annealing defects can be considered as a phase change reaction, which may be described using kinetic models [21-24]. Previous graphite annealing models have used data obtained from neutron-irradiated graphite samples. This work uses kinetic models to describe the annealing process in ion-irradiated graphite. Data from the experiments has been used to derive the kinetic model activation energies and characteristic functions. The objective is to show that thermal annealing of graphite defects can be understood through the use of kinetic modelling to determine the activation energy E_a and pre-exponential factor A in the Arrhenius equation. The activation energy is a measure of the energy barrier to be overcome in order for the annealing reaction to progress.

The basic relationship that all kinetic approaches use is defined as [21-28]:

$$\frac{dx}{dt} = kf(x) \quad (2)$$

where x is a variable that is described by the Arrhenius distribution, $f(x)$, using a linear increase in time to characterize the sample, and k is a constant of proportionality. Various forms of the function $f(x)$ have been considered, such as $f(x) = x^n$ which is used to consider a reaction of n^{th} order or the more complex $f(x) = x^n (1-qx)^m$ [28].

The objective of these methods is to obtain the activation energy E_a , and pre-exponential factor A , for each process as expressed in the form of a standard Arrhenius equation:

$$k = A \exp\left(\frac{-E_a}{RT}\right) \quad (3)$$

where

k = the rate of reaction (specific rate)

A = Arrhenius factor or pre-exponential factor. This typically is a frequency factor referring to number of collisions per second. In the case of the annealing reaction, the number of reacting (vanishing or moving) defects per second is analogous.

E_a = energy of activation, expressed in Joule/mol

R = universal constant for an ideal gases ($8.314 \text{ m}^2 \text{ kg s}^{-2} \text{ K}^{-1} \text{ mol}^{-1}$)

T = absolute temperature (Kelvin)

The process of annealing defects is assumed to be a reaction, and as such obeys the laws of thermodynamics and chemical kinetics (strictly, the annealing of defects resembles mostly a change of phase due to the increased mobility of defects).

Consequently the rate of reduction of defect quantity Q follows an Arrhenius law:

$$\frac{dQ}{dt} = A e^{\frac{-E_a}{RT}} Q^n \quad (4)$$

Where :

Q = the quantity of defects at a given state of the annealing at time t

The reaction order n in the case of a chemical reaction is the relation between reactants and compounds; in the case of annealing of defects it is used a similar way to describe the recombination or reordering of defects. It is also to be expected that n may be affected by other parameters such as diffusion, rate of heating, microstructure characteristics, or the general condition of sample and experimental conditions. Some authors [23] have used the function $f(x) = x^n$ or $f(Q) = Q^n$ to describe the annealing of defects in graphite to analyse results obtained using Differential Scanning Calorimetry (DSC).

By solving the differential equation in Equation 4 we obtain:

$$dQ = Ae^{\frac{-E_a}{RT}} Q^n dt \quad (5)$$

thus by replacing

$$dT = a dt \quad (6)$$

where a is the heating rate, we obtain:

$$dQ = \frac{A}{a} e^{\frac{-E_a}{RT}} Q^n dT \quad (7)$$

The solution of this differential equation can give the quantity of defects as a function of temperature or time:

$$Q = \left[1 - \frac{Ae^{\frac{-E_a}{RT}} (-1+n)T}{a} \right]^{\frac{1}{1-n}} \quad (8)$$

A graphic form of Equation (8) is given in Figure 6 (normalized quantities).

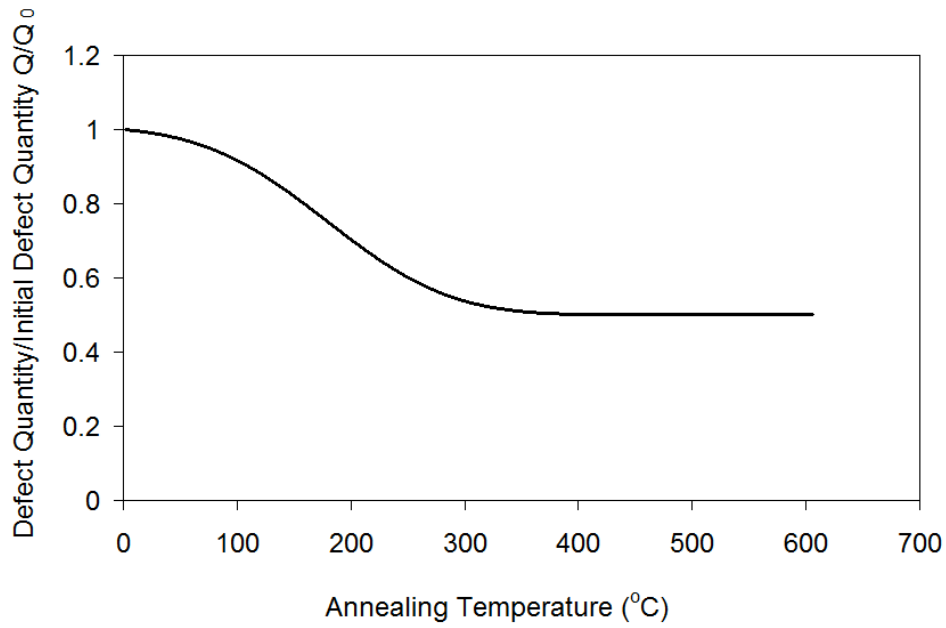


Figure 6. The defect quantity Q at temperature T normalised by the initial defect quantity Q_0 . Graphical depiction of Equation 8

In Figure 6 it can be observed that the shape of this relationship resembles the variation of I_D/I_G versus annealing temperature obtained from Raman spectroscopy (Figure 5). This suggests that the variation of the I_D/I_G ratio may be described in terms of annealing of the quantity of defects.

A more useful quantity utilized further in the present work is the portion of the defect quantity that was annealed at every temperature, $\%q$, which is obtained from the

existing proportion of defects Q , the final remaining quantity Q_∞ , the initial Q_0 and the final proportion of defects Q_∞ :

$$q = \left(\frac{Q - Q_\infty}{Q_0 - Q_\infty} \right) \quad (9)$$

The divergence between calculated and experimental results, can be expressed as a percentage, associated with the largest rate of reaction observed in the experimental curve, of the following type [24, 25, 27]:

$$Dev1(\%) = 100 \frac{\sqrt{SUM_Q / (Z - N)}}{\max[(q)^{exp}]} \quad (10)$$

Where Z is the total number of measurements used to represent the curve and N is the number of parameters that were used in the model, i.e. activation energy E_a , pre-exponential factor A , and order of reaction n . The parameter $(q)^{exp}$ refers to the normalized quantity of defects as calculated by the I_D/I_G ratio (i.e. Figure 5).

In this work, the parameter N was excluded due to the small number of measurements, thus Equation 10 becomes:

$$Dev1(\%) = 100 \frac{\sqrt{SUMq / (Z)}}{\max[(q)^{exp}]} \quad (11)$$

The parameter SUM_Q can be described as:

$$SUM_Q = \sum_{i=1}^N \left[\left((q_i)^{exp} \right) - \left((q_i)^{calc} \right) \right]^2 \quad (12)$$

$(q)^{calc}$ refers to the normalized quantity of defects, obtained using the fit to data.

Minimising the parameter $DevI$ is a non-linear optimization problem, and can be solved using a nonlinear optimization algorithm [24, 25, 26, 28] by controlling the activation energy E_a , pre-exponential factor A , and order of reaction n ; these are the kinetic parameters. The solution is generally considered satisfactory when $DevI$ is less than 3% [24, 25, 26, 28]. In this work, the Generalized Reduced Gradient [29] implemented within the Solver Add-in of Microsoft Excel 2003, was utilized.

Previous researchers [21,22, 30, 31], using variations of the above equations, conducted kinetic analysis on neutron-irradiated graphite samples taken from British and Japanese nuclear reactors. These samples were annealed using Differential Scanning Calorimetry (DSC). During annealing, measurable amounts of energy are released from the graphite samples. This phenomenon, also known as Wigner energy release, is the release of accumulated energy that was stored in the graphite in the form of potential energy, during the irradiation. DSC experiments provide data on the rate of energy release in a specimen versus temperature or time. Wigner energy [16,21-24] is the potential energy of the carbon atoms that have been displaced from their original lattice position by neutron bombardment such as takes place a nuclear reactor. The population of defects Q is proportional to the energy released S .

$$Q = \lambda' \cdot S \quad (13)$$

where λ' is a proportionality factor.

Thus the population of defects in a neutron-irradiated sample can be characterized by analyzing the Wigner energy release data, measured in a DSC experiment.

The usual equations that are used to describe Wigner energy release are presumed to follow also an Arrhenius law [28]: For example, in a DSC experiment where the temperature rises linearly, the release of stored energy is given by:

$$\frac{dS}{dt} = A \exp\left(\frac{E_a}{RT}\right) S^n \quad (14)$$

where S is the energy released, and n the reaction order; these are the same kinetic parameters as used in the Equation (8). Therefore, by measuring Wigner energy release by DSC, and by measuring the I_D/I_G ratio in a Raman experiment, two different aspects of the same phenomenon may be monitored; that is the reduction of the defects due to thermal annealing.

Consequently by analyzing DSC data from neutron-irradiated graphite, and Raman data from ion-irradiated graphite, a comparison between the annealing processes of ion irradiation and neutron irradiation is achievable, since both refer to restoration of damage. Previous researchers [21, 22, 30, 31] applied a similar kinetic algorithm to DSC data that had been obtained from neutron-irradiated nuclear grade graphite, but not ion-irradiated graphite. In this paper a comparison is made between the annealing processes obtained by analysis of DSC data from neutron-irradiated graphite, and Raman data from ion-irradiated graphite.

The Arrhenius equations that have been described above can be applied to experiments with constant heating rate. During a continuous heating as such, thermal lagging phenomena occur, and the completion of the annealing reaction appears to terminate at temperatures higher than actual. Therefore a drift of the annealing graph towards higher temperatures takes place. The extent of this drift is exponentially

dependent upon the heating rate, as is shown in equations 7 and 8. Consequently these equations are strictly unsuitable to analyse this work's experimental data that describe stepwise annealing. In the thermal graphs of this work, at every I_D/I_G versus temperature point the annealing reaction is considered to have been completed and no thermal drift takes place.

However, a continuous annealing experiment under a very low heating rate, at around $1^\circ\text{C}/\text{min}$, should allow sufficient time for the annealing reaction to complete. Then, during the course of the annealing, the reaction completion rate would coincide with heating rate. So, no thermal lagging occurs and the graph drift becomes insignificant. Consequently, in the analysis that follows the I_D/I_G points derived after heating and cooling at each temperature level, could be considered to coincide with a continuous single annealing plot under a very low but constant heating rate. Therefore stepwise annealing could be simulated by continuous annealing. The heating rate was an additional parameter during optimization and an optimum value of about $1.4^\circ\text{C}/\text{min}$ was calculated and used in the present work.

3.1.1 Single reaction kinetic model (neutron damage)

Simmons [21] tested a constant activation energy kinetic model, which assumed that activation energy remained constant over the temperature range of the release.

$$\frac{dS}{dt} = S.A \exp\left(-\frac{E}{kT}\right) \quad (15)$$

Nightingale [23] proposed a model based on the assumption of constant frequency/constant activation energy and introduced the order of the reaction, n , as an

additional variable. He assumed that there can be an order of reaction different from unity and estimated it to be around 6-8.

$$\frac{dS}{dt} = S^n A \exp\left(-\frac{E}{kT}\right) \quad (16)$$

The constant activation energy model has been discussed in detail in [32]. For comparison this paper analyses the I_D/I_G data using the Simmons general model and the Nightingale model. The scope of this examination was to identify the proximity of the Simmons and Nightingale scenarios to the experimental curves derived in this study, in order to assess if there was a need of further analysis with more complicated scenarios.

3.1.2 Multiple reaction kinetic models (neutron damage)

Other researchers have interpreted the Wigner energy release reaction using multiple reactions [22, 30, 31]. The more characteristic analyses include that of Kelly et.al [31] who proposed a three reactions model, assuming three first order reactions were taking place with the same pre-exponential factor. More recently Lexa et.al [30] studied the release of Wigner energy from graphite irradiated by fast neutrons at a TRIGA Mark II research reactor. They examined a model with four first order reactions also with the same pre-exponential factor. Iwata [22] irradiated specimens of pyrolytic graphite at the JAERI JRR-2 experimental reactor in Japan and proposed a model with three first order reactions, but using different pre-exponential factors. All these studies, including that of Lexa et.al [30], assume first order reactions. With the exception of Iwata [22] these authors did not numerically assess the efficiency of their simulations.

The values of activation energy and pre-exponential factors taken from the studies referred to above, for both single reaction kinetic models and multiple reaction kinetic models are presented in Table 1. All of them found the first reaction to have an energy of 1.2 to 1.5 eV, whilst the second reaction was found by all to be around 1.5 eV with less variation. The third reaction was found between 1.6 to 1.8 eV, while Lexa et al [30] claimed the existence of an additional fourth reaction at 1.7 eV. These reactions have been assumed by Lexa et al [30] to refer to sequences of combinations of vacancy interstitial migrations and annihilations.

	1st Reaction			2nd Reaction			3rd Reaction			4th Reaction		
	n	A(1/sec)	E _a (eV)	n	A(1/sec)	E _a (eV)	n	A(1/sec)	E _a (eV)	n	A(1/sec)	E _a (eV)
Simmons [17]	Constant Activation Energy Model		1.2	General Model		1.2						
Iwata [18]	1	6.2x10 ⁸	1.4	1	2.4x10 ⁹	1.5	1	4.2x10 ¹⁰	1.8			
Lexa et.al. [26]	1	7.5x10 ¹³	1.3	1	7.5x10 ¹³	1.5	1	7.5x10 ¹³	1.6	1	7.5x10 ¹³	1.7
Kelly et. al. [27]	1	7.5x10 ¹³	1.5	1	7.5x10 ¹³	1.5	1	7.5x10 ¹³	1.8			

Table 1. Activation energy and pre-exponential factors due to Simmons [21], Iwata [22], Lexa et.al [30] and Kelly et. al, [31].

3.1.3 Single reaction kinetic models: Ion and mechanical damage

Based on the assumptions of Simmons [21] and Nightingale [23], a single reaction kinetic model was applied to the Raman data for ion and mechanical damage. To investigate the single reaction model, Equation (8) was fitted to the experimental results for the consecutive annealing and Raman spectroscopy on ion-irradiated and mechanically polished graphite.

The model can be described as a single reaction kinetic model, as it is based on the assumption that the annealing process can be simulated by one reaction. Therefore only one set of values of A , E_a , and n have to be calculated,

The results from the fitting process are shown at Table 2 and Figure 7.

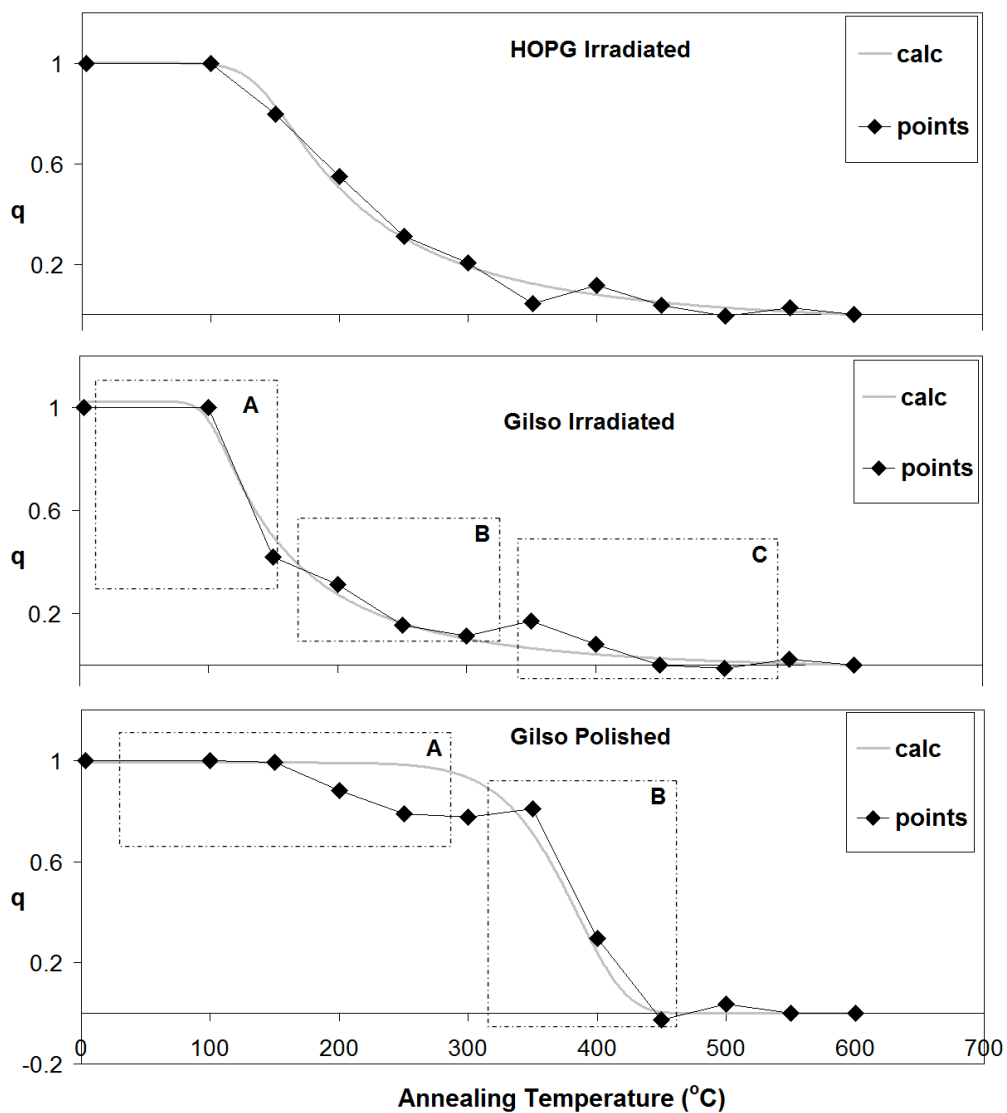


Figure 7. HOPG irradiated with Ar ions (top) Gilsocarbon irradiated with Ar ions (middle) , and Gilsocarbon polished (bottom): Scenario with one reaction

	H.O.P.G Ar+	Gilso Ar+	Gilso Polished
A (1/sec)	1.73×10^8	3.40×10^{18}	7.65×10^3
E(eV)	1.0	1.6	0.9
n	6.7	10.0	1.0
Dev1(%)	3.3	4.6	8.6

Table 2: Summary of results for the single reaction kinetic model analysis

Figure 7 shows the remaining fraction, q , of defects versus the annealing temperature obtained by this analysis. The results were satisfactory for the data derived from the annealing of ion-irradiated HOPG. For HOPG the value of $Dev1$ reached a minimum of 3.3 and the model convergence criteria were almost satisfied. The other two sets of data, from ion-irradiated and polished Gilsocarbon did not achieve satisfactory convergence, and the values of $Dev1$ in both cases exceeded 3% at 4.6% and 8.6% respectively.

A comparison between the previous researchers' DSC kinetic analysis on neutron-irradiated graphite and Raman peaks kinetic analysis shows that the values for E_a and n are not in close agreement. As noted earlier, Simmons [21], Iwata [22], Lexa [30] and Kelly [31] found activation energies of the order of 1.2 to 1.5 eV whereas in this work, for ion-irradiated HOPG, and mechanically polished Gilsocarbon, the activation

energy was around 1.0 and 0.9 eV respectively. The reaction order n reported by Nightingale [23] for neutron-irradiated graphite was between 6 to 8, which is in agreement with the value of 6.7 calculated in this work for ion-irradiated HOPG. However, for ion-irradiated and mechanically polished Gilsocarbon the values of n lay outside these limits (10 and 1 respectively).

It can be concluded that the single reaction model does not adequately fit the experimental I_D/I_G data presented here. This is indicative of the inadequacy of the model; there should be some agreement between the kinetic parameters obtained for ion-irradiated Gilsocarbon, and ion-irradiated HOPG. These two different types of graphite receive exactly the same fluence and type of irradiation, therefore the damage induced would be expected to be similar in terms of quality. This is supported by their similar Raman spectra (e.g. Figure 1). Their annealing kinetic parameters would not be expected to vary significantly, thus more complex scenarios are examined as described below.

3.2 Independent parallel reactions model

The assumption that more reactions take place during the annealing process is not new. This has been proposed by Kelly et.al [31], Iwata [32], and Lexa et.al [30], for neutron induced damage and therefore needs to be considered for ion irradiation damage as well.

Researchers have used the independent parallel reactions model to study heterogeneous reactions in biomass and fossil fuels [25, 26]. These models presuppose the existence of independent parallel reactions without interactions between them. For this particular analysis the independent reactions, also called partial

reactions or “pseudo-reactions”, that can take place sequentially implying that each pseudo-reaction begins either when another finishes, or in parallel supposing that pseudo-reactions develop simultaneously, without interactions. Combinations of these two possibilities can also be selected for the analysis of more complex systems.

In the multiple reactions approach of the analysis of defects, it is assumed that the overall result is the sum of each reaction:

$$q = \sum_i q_i \quad (17)$$

where q_i are the individual reactions taking place. The summation of the q_i produces an overall result of the reduction in the quantity of defects given by:

$$q_i = \int_{T_0}^T \left[1 - \frac{A_i e^{\frac{-E_{ai}}{RT}} (-1 + n_i) T}{a} \right]^{\frac{1}{1-n_i}} \quad (18)$$

where q_i is the reduction in the quantity of defects from an individual partial reaction.

The application of the independent parallel reactions model to the annealing of defects, due to its complexity, can provide a variety of scenarios for a single set of data. There are some general guidelines [24-26, 28] for the use and acceptance of results from a kinetic analysis scenario. In summary these are: A model is considered valid when fitted to one set of experimental data can predict another independent set of data; In general the simplest model available should be chosen; Results between different experiments may vary slightly, so it is considered essential that they produce results of the same order; The shape of the predicted curve must follow the

experimental data, since even when the target of $DevI < 3\%$ is achieved, the shapes of experimental and calculated curves can still show significant differences when the model is incorrect.

In the independent parallel reactions model, a parameter that refers to the percentage of participation of each partial reaction to the overall process is included. This parameter, c , is explained in detail elsewhere [24]. As a result, four parameters take part in the optimization process for each partial reaction, namely the activation energy E_a , the pre-exponential factor A , the order of reaction n , and percentage of participation c .

Two possible scenarios are examined here for the ion-irradiated and mechanically damaged samples. In the first, the intensity ratio and the normalized intensity ratio were assumed to be directly proportional to the quantity of defects, as before. In the second, a non-linear square root dependence was examined.

3.2.1 Scenario I. Linear relation between quantity of defects and

$$I_D/I_G$$

The previous researchers [22, 30, 31] used a kinetic approach scenario of three partial reactions. In this work, based on the above equations, and the assumption that the relationship between defect quantity and I_D/I_G is linear, a three partial reactions model was chosen and applied to the ion-irradiation and mechanical damage data. The starting point values of the optimization were chosen from Table 1, and the results from this analysis are given in Figure 8 and on Table 3.

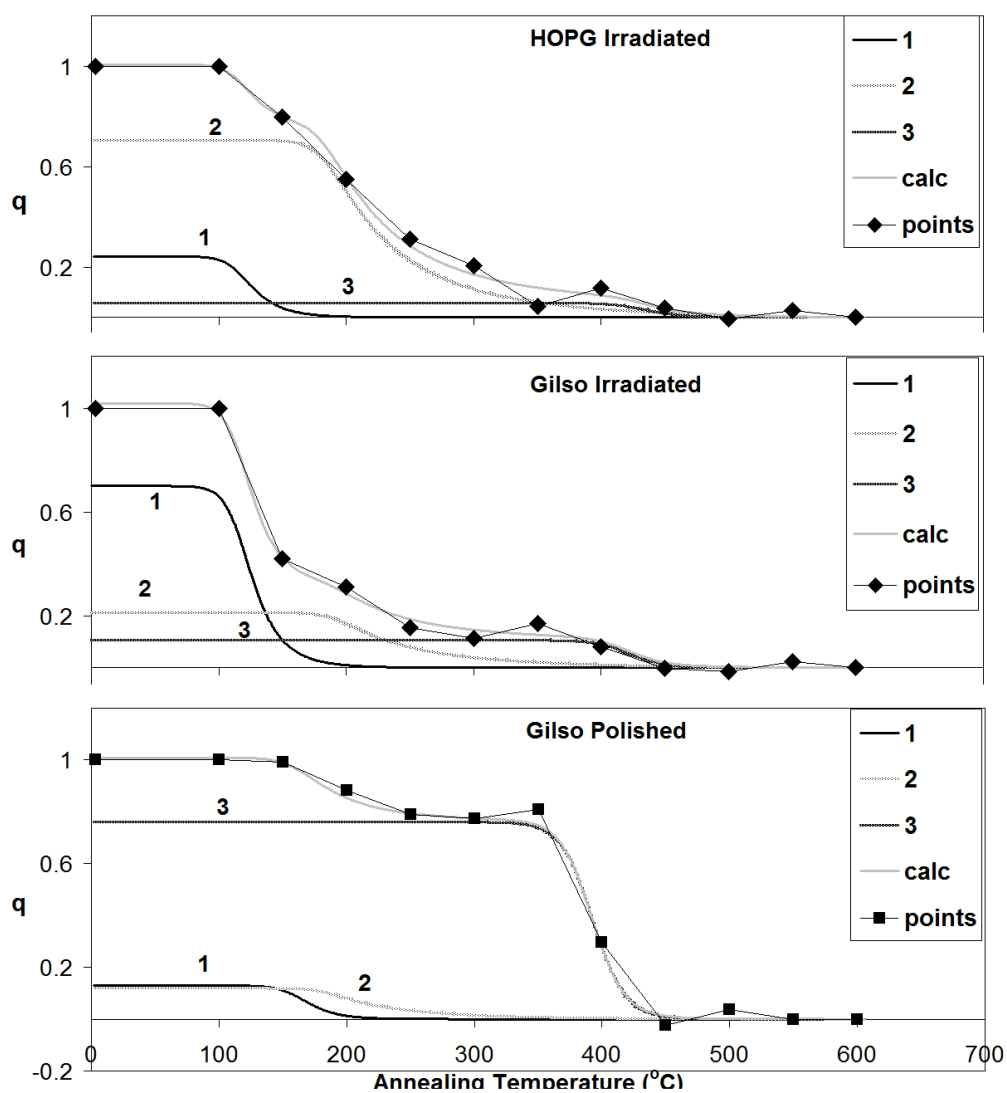


Figure 8. HOPG irradiated with Ar ions (top) Gilsocarbon irradiated with Ar ions (middle), and Gilsocarbon polished (bottom): Scenario with three reactions

H.O.P.G Ar+	1st reaction	2nd reaction	3rd reaction	Dev1 (%)
A (1/sec)	8.7×10^{15}	8.2×10^{16}	3.3×10^{17}	
E(eV)	1.5	1.9	2.9	2.8
n	2.9	6.8	2.0	
c(%)	24	72	6	

Gilso Ar+	1st reaction	2nd reaction	3rd reaction	Dev1 (%)
A (1/sec)	1.7×10^{16}	6.3×10^{16}	1.7×10^{18}	
E(eV)	1.5	1.9	2.9	2.5
n	2.9	6.8	2.0	
c(%)	70	22	11	

Gilso Polished	1st reaction	2nd reaction	3rd reaction	Dev1 (%)
A (1/sec)	1.7×10^{14}	1.7×10^{17}	1.7×10^{19}	
E(eV)	1.5	1.9	2.9	2.6
n	2.4	6.1	2.0	
c(%)	13	12	76	

Table 3: Overall results for the three reactions (Scenario 1).

The activation energies for the three reactions have been calculated as 1.5, 1.9 and 2.9 eV respectively. The first two reactions are in accordance with the second and the third reaction values reported by Iwata [22], Lexa et.al [30] and Kelly et.al [31]. The third reaction exceeds these values, but for the ion-irradiated HOPG and Gilsocarbon does not have a very high contribution (i.e. c); this implies that there is not high confidence in its contribution to this model. The first reaction obtained by Iwata [22], Lexa et.al [30] and Kelly et.al [31] for neutron irradiation is not found in the analysis of these data. This implies that neither ion irradiation nor mechanical processes create defects that anneal at such low temperatures.

The values of the reaction orders calculated for all reactions exceed unity. However they are the same for all three sets of experiments, which is an indication that they can be considered as reproducible and characteristic. The value of the reaction order n for the second reaction is higher than the first and the third reactions. However, these values are in accordance with values reported by Nightingale [23] of between 6 to 8.

From Table 3 it can be seen that the third reaction for ion-irradiated Gilsocarbon and HOPG does not have the same high contribution as found for polished Gilsocarbon (the contribution c was 6 and 11% for ion-irradiated Gilsocarbon and HOPG respectively). This implies that there is low confidence in the values obtained, indicating that the third reaction may be omitted. However, since this third reaction is prominent in the annealing characteristic of polished Gilsocarbon, it may exist and an overall three reaction scenario basis is possible. Such a scenario has also been proposed in the literature [22, 30, 31], however, its existence is subjective and the authors suggest that further research would be required to substantiate it. It is also possible that the annealing of polished Gilsocarbon can be interpreted by a two reactions model and the first two reactions between 0 to 250°C may be merged. To investigate this the third reaction was omitted in an analysis of the ion-irradiated specimens; in the case of the polished Gilsocarbon the second reaction was omitted and the first is expanded to contain the uncovered territory. The results are presented in Table 4 and Figure 9.

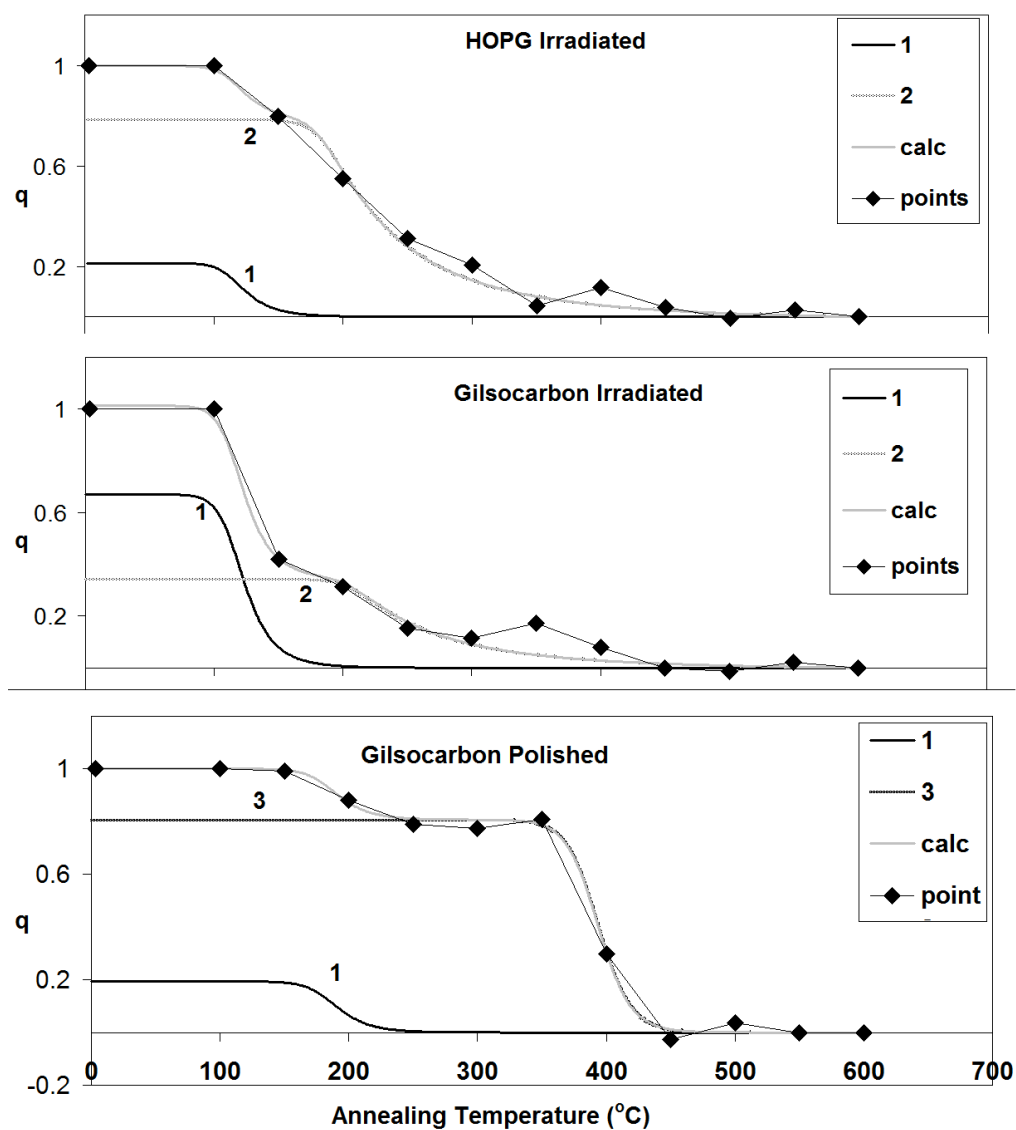


Figure 9. HOPG irradiated with Ar ions (top) Gilsocarbon irradiated with Ar ions (middle) , and Gilsocarbon polished (bottom): Scenario 1 with two reactions

H.O.P.G Ar+	1st reaction	2nd reaction	3rd reaction	Dev1 (%)
A (1/sec)	1.5×10^{18}	1.4×10^{17}	-	
E(eV)	1.5	1.9	-	3.3
n	2.9	7.3	-	
c(%)	21	80	-	

Gilso Ar+	1st reaction	2nd reaction	3rd reaction	Dev1 (%)
A (1/sec)	1.7×10^{18}	6.3×10^{18}	-	
E(eV)	1.5	1.9	-	4.2
n	2.8	7.3	-	
c(%)	67	35	-	

Gilso Polished	1st reaction	2nd reaction	3rd reaction	Dev1 (%)
A (1/sec)	1.7×10^{14}	-	1.7×10^{19}	
E(eV)	1.6	-	2.9	2.0
n	2.4	-	2.0	
c(%)	19	-	81	

Table 4: Summary of results for the two reactions analysis (Scenario 1).

In the case of HOPG, *Dev1* was found to be marginally outside of the acceptable limits and for ion-irradiated Gilsocarbon the overall score was worse (4.2%). However for polished Gilsocarbon there was a major improvement (2.0 % for the two reactions against 2.6 for the three reactions, which improves the fit).

3.2.2 Scenario 2 – Square root relation between quantity of defects and I_D/I_G

Kitajima et al. [33] and Asari et al. [34, 35] have produced a model where the quantity of defects is proportional to the square root of the relative intensity ratio. Their approach was based on the several assumptions. Firstly, the mean distance L between

the in-plane defects is proportional to the square root of the quantity of defects within a graphitic layer Q_L .

$$L = (Q_L)^{-\frac{1}{2}} \quad (19)$$

Secondly, there is no interaction between the layers during the production of the defects. The produced defects are distributed between the layers and the interstitial atoms do not bridge the gap between them (It is noted that Li et al. [36] claim the opposite, stating that there are cases where interstitial atoms come to rest to pre-defined positions between the layers).

Following the assumptions of Kitajima et al. [33] and Asari et al. [34, 35], the quantity of defects produced Q_D can be expressed as a linear function of the in-layer defects Q_L :

$$Q_L = fQ_D \quad (20)$$

Where $f=0.335$ nm, i.e. the distance between the graphitic layers

It is also assumed that the in-plane phonon correlation length L_a corresponds to the mean distance L between the defects.

Consequently, since the in-plane phonon correlation length is related to the relative intensity ratio of the D to G mode, as is given by the relation below [37]:

$$\frac{I_D}{I_G} = \frac{C(\lambda)}{L_a} \quad (21)$$

(for a wavelength of $\lambda=514.5$ nm and an optical depth of $C(\lambda)=4.4$ nm)

where the quantity of defects per layer N_L can be correlated with the relative intensity ratio as:

$$\frac{I_D}{I_G} = C(\lambda)\sqrt{Q_L} \quad (22)$$

By combining Equation (22) with (20) the overall defect quantity is expressed as

$$Q_D = \frac{1}{fC^2(\lambda)} \left(\frac{I_D}{I_G} \right)^2 \quad (23)$$

Consequently, the normalized quantity q becomes:

$$q = \left(\frac{Q - Q_\infty}{Q_0 - Q_\infty} \right) = \left[\left(\frac{I_D}{I_G} \right)^2 - \left(\frac{I_D}{I_G} \right)_\infty^2 \right] / \left[\left(\frac{I_D}{I_G} \right)_0^2 - \left(\frac{I_D}{I_G} \right)_\infty^2 \right] \quad (24)$$

When applied to the kinetic parameter algorithm, the calculated results better fit the experimental values (Figure 10 and Table 5). The values of $Dev1$ for all ion-irradiated

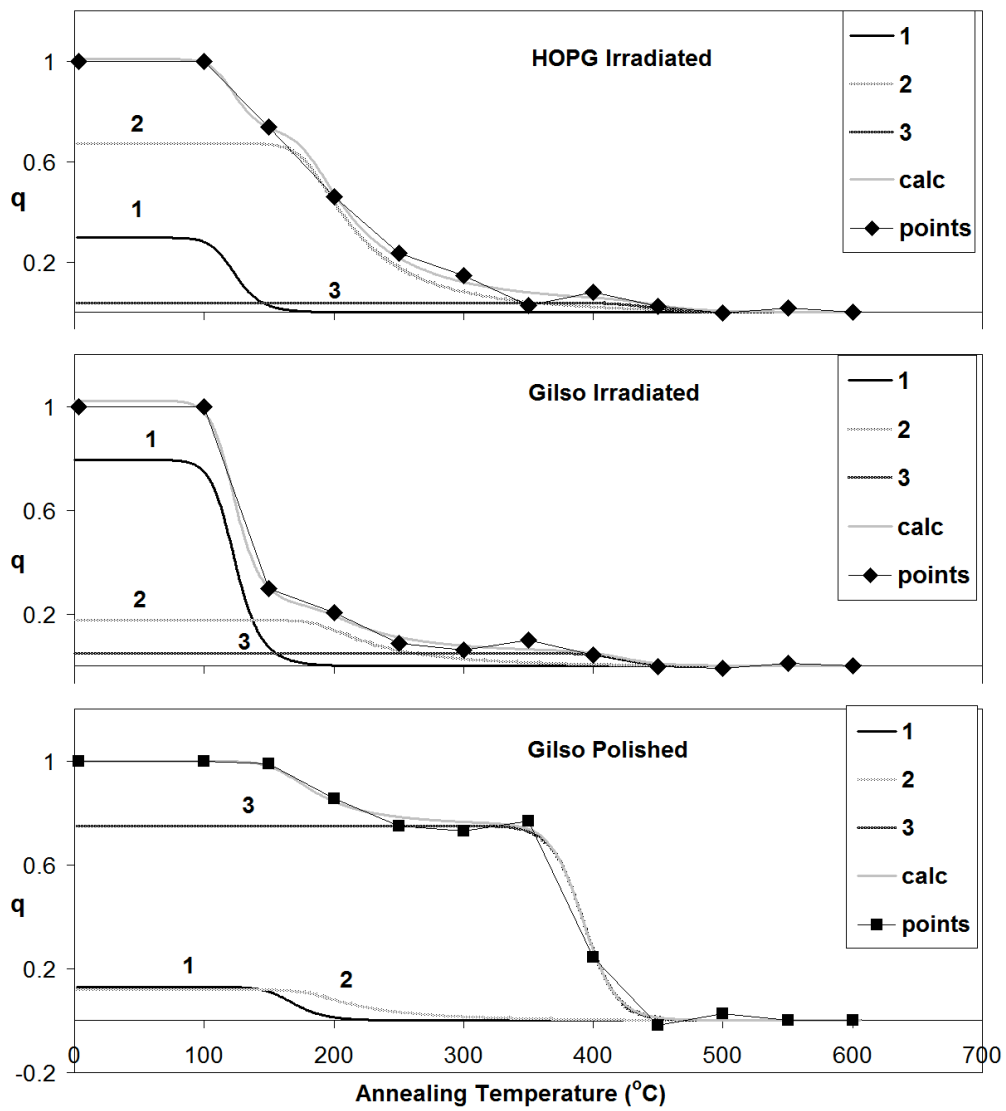


Figure 10. HOPG irradiated with Ar ions (top) Gilsocarbon irradiated with Ar ions (middle) , and Gilsocarbon polished (bottom): Scenario 2 with three reactions and assumption of square root proportionality

HOPG and Gilsocarbon ion-irradiated and polished are 2, 1.8 and 2.2

H.O.P.G Ar+	1st reaction	2nd reaction	3rd reaction	Dev1 (%)
A (1/sec)	8.7×10^{15}	1.2×10^{17}	1.7×10^{17}	
E(eV)	1.5	1.9	2.9	2.0
n	2.4	6.1	2.0	
c(%)	30	68	4	

Gilso Ar+	1st reaction	2nd reaction	3rd reaction	Dev1 (%)
A (1/sec)	1.7×10^{16}	6.3×10^{16}	1.7×10^{18}	
E(eV)	1.5	1.9	2.9	1.8
n	2.4	6.1	2.0	
c(%)	79	18	5	

Gilso Polished	1st reaction	2nd reaction	3rd reaction	Dev1 (%)
A (1/sec)	1.7×10^{14}	1.7×10^{17}	1.7×10^{19}	
E(eV)	1.5	1.9	2.9	2.3
n	2.4	6.1	2.0	
c(%)	13	12	75	

respectively

Table 5: Overall results for the scenario of the three reactions, with the assumption of square root proportionality (Scenario 2).

compared to 2.8, 2.5 and 2.6 for scenario I. The values of activation energies remain the same and the reaction orders decrease slightly. In all the models tested the first two reactions with activation energies of 1.5-1.6 and 1.8-1.9 eV due to Iwata [22] correspond to that of a di-interstitial annihilated by two mono-vacancies. Reynolds [38] proposes that an activation energy estimate of 1.8 to 2.6 eV corresponds to mobilization of defect aggregates and Telling et al. [39], amongst other authors, proposes that a 1.7 eV activation energy corresponds to vacancy migration.

The assumption of Kitajima et al. [33] and Asari et al. [34,35], that the quantity of defects is proportional to the square root of the relative intensity ratio, produces better results, and is consistent with other Raman Spectroscopy studies [20, 40, 41]; however their assumption can not obviously rule out the existence of interactions between the layers during the production of the defects. Bonding between layers by irradiation induced interstitials in double walled carbon nanotubes have been observed in TEM studies [42] and their annealing characteristics have also been monitored. Therefore the observed reduction of I_D/I_G might also imply annealing of intralayer bonding. Analyses that are more sensitive to the structure and arrangement of defects than those considered here are needed to resolve this issue.

In both of the scenarios, despite the calculated activation energies being close to values reported by literature, the pre-exponential factors are higher (Table 3). It therefore can be assumed that ion irradiation can describe the same phenomenon as neutron irradiation in qualitative but not in quantitative terms, therefore pre-exponential factors may be expected to vary. The defects introduced by ion irradiation, mechanical damage and neutron irradiation were found to anneal with the similar activation energies, but are in different proportions (as shown by the reaction orders and relative contributions). There may also be synergies between the defect types that are not revealed by this analysis. This is even more evident in the case of annealing defects produced by mechanical polishing, by comparing the overall contribution of each reaction with the ion-irradiated sample scenarios. Therefore the annealing processes for ion irradiation-induced damage tested in this work, and neutron irradiation-induced damage reported in literature do differ. However, there is an overall qualitative resemblance between the calculated kinetic parameters derived

in this work for ion irradiation data, and a combination of the kinetic scenarios that have been reported in the literature.

In the scenario 2 analysis, the third reaction (Table 5) does not contribute highly for ion-irradiated Gilsocarbon and HOPG, similarly to the Scenario 1. A further analysis was carried out, omitting the third reaction, which resulted in contributions within acceptable limits (2.4 and 2.5 for HOPG and ion-irradiated Gilsocarbon respectively). Hence, with the assumption of no interaction between the layers during the production of the defects, a simpler two-reaction scenario 2 model is capable of producing adequate results, contrary to scenario 1. In the case of polished Gilsocarbon, a two reaction fit was implemented by merging the first two reactions, as was examined for scenario 1. The deviation was reduced by 0.2%. The results are shown in Figure 11 and in Table 6

H.O.P.G Ar+	1st reaction	2nd reaction	3rd reaction	Dev1 (%)
A (1/sec)	8.8×10^{15}	1.2×10^{17}	-	
E(eV)	1.5	1.8	-	2.4
n	2.2	6.6	-	
c(%)	31	70	-	

Gilso Ar+	1st reaction	2nd reaction	3rd reaction	Dev1 (%)
A (1/sec)	1.7×10^{16}	6.3×10^{16}	-	
E(eV)	1.5	1.9	-	2.5
n	2.2	6.6	-	
c(%)	78	23	-	

Gilso Polished	1st reaction	2nd reaction	3rd reaction	Dev1 (%)
A (1/sec)	1.7×10^{14}	-	1.7×10^{19}	
E(eV)	1.6	-	2.9	2.1
n	2.4	-	2.0	
c(%)	26	-	76	

Table 6 Overall results for the scenario of the two reactions, with the assumption of square root proportionality (Scenario 2).

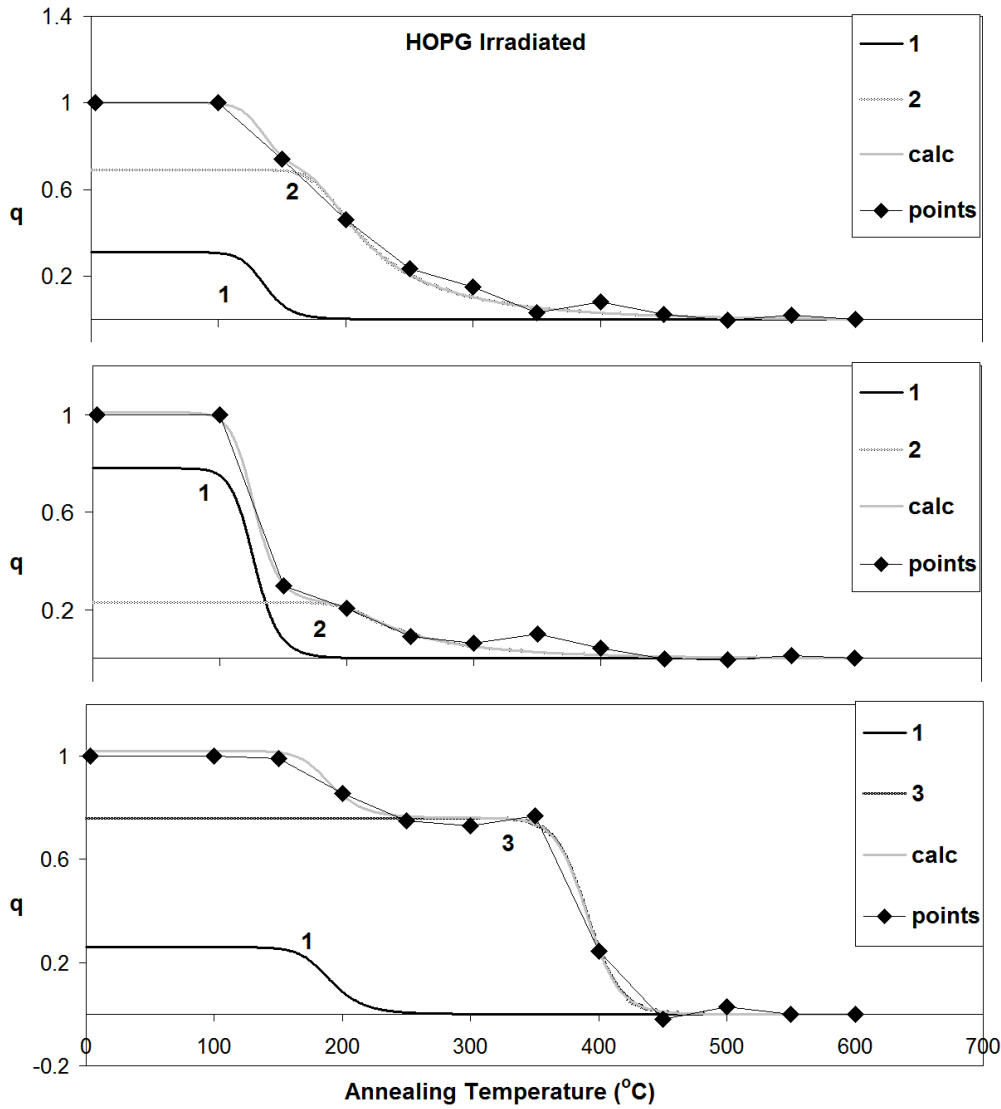


Figure 11 HOPG irradiated with Ar ions (top) Gilsocarbon irradiated with Ar ions (middle) , and Gilsocarbon polished (bottom): Scenario with two reactions and assumption of square root proportionality.

4 Conclusions

The kinetic analysis of the annealing of ion-irradiated and polished graphite samples and the investigation of the decrease of the Raman I_D/I_G ratio has been used to interpret the annealing process as a convolution of two and possibly three different processes, using an independent parallel reactions kinetic model. The magnitudes of these processes differ in the two types of damage.

The two or three reaction analysis provides a better fit the data than the assumption of a single reaction. An assumption that I_D/I_G is proportional to the square root of the defect quantity produces better fits than the assumption of a linear dependence.

The ability to interpret the annealing reaction of an ion-irradiation technique with a kinetic scenario that has previously used for stored energy release from neutron-irradiated specimens indicates qualitative similarities between ion and neutron irradiation. Ion irradiation, together with Raman spectroscopy, therefore has the potential to provide insight into irradiation neutron damage annealing in nuclear graphite.

Acknowledgements.

The authors wish to express gratitude to the Greek State Scholarships Foundation for financial and laboratory expenses support. They would also wish to express gratitude to British Energy Generation Ltd. for the supply of non-irradiated (virgin) Gilsocarbon specimens and the UKAEA (United Kingdom Atomic Energy Authority) for the supply of neutron-irradiated BEPO graphite with the permission of UK NDA (Nuclear Decommissioning Authority).

References

- [1] Asari E, Nakamura K G, Kawabe T, Kitajima M.. J Nuc Mater, 1997; 244, 173-175.
- [2] Asari E. Carbon 2000; 38, 1857–1861.
- [3] Liu J, Yao H J, Sun Y M, Duan J L, Hou M D, Mo D, Wang Z G, Jin Y F, Abe H, Li Z C, Sekimura N. Nucl Instrum Meth B. 2006; 245, 126–129.
- [4] Compagnini G, Puglisi O, Foti G. Carbon 1997; 35, 1793-1797.
- [5] Ishioka K, Hase M, Ushida K, Kitajima M. Physica B 2002; 316–317, 296–299.
- [6] Liu J, Hou M D, Trautmann M, Neumann C R, Muller C, Wang Z G, Zhang Q X, Sun Y M, Jin Y F, Liu H W, Gao H J. Nucl Instrum Meth B. 2003; 212, 303–307.
- [7] Niwase K.. Mat Sci Eng A Struct 2005; 400–401, 101–104.
- [8] Hida A, Meguro T, Maeda K, Aoyagi Y. Nucl Instrum Meth B. 2003; 205, 736–740.
- [9] Hall G, Marsden B J, Fok S L. J Nucl Mater 2006; 353, 12-18.
- [10] Brülle T, Stimming U. J Electroanal Chem 2009; 636, 10-17.
- [11] Ziegler J F, Ziegler M D, Biersack J P. Nucl Instrum Meth B. 2010; 268, 1818-1823
- [12] Borisov A M, Mashkova E S, Nemov A S, Virgiliev Y S. Nucl Instrum Meth B. 2007; 256, 363–367.

- [13] Asari E, Kitajima M, Nakamura K G. Carbon 1998; 36, 1693–1696.
- [14] Ferrari A C, Robertson J. Phys Rev B 2000; 61, 14095-14107
- [15] Nakamizo M. Tamai K. Carbon 1984; 22, 197-198.
- [16] Dickson J L, Kinchin G H, Jackson R F, Lomer W, Simmons J H W. BEPO Wigner energy Release. A- U.K Atomic Energy Authority, A.E.R.E. Harwell. Second United Nations International Conference on the Peaceful Uses of Atomic Energy. A/Conf.15/P/1805. United Kingdom. 13 June 1958.
- [17] T. Hirai, J. Compan, K. Niwase, J. Linke, J. Nucl. Mater.373 (2008), 119.
- [18] A.Theodosiou, A.F. Carley, S.H. Taylor, J. Nucl. Mater.403 (2010), 108.
- [19] K. Niwase, I. Tanaka, T. Tanabe, J. Nucl. Mater. 191-194 (1992) 335.
- [20] K. Niwase, Phys. Rev. B, 52 (1995) 15785.
- [21] Simmons J H W. AEA Technology. AEA RS 5283. March 1994.
- [22] Iwata T. J Nuc Mater 1985; 133-134, 361-364.
- [23] Nightingale R E.TID-7565(Pt.1) Dec. 1957 US/UK Graphite Conference St., Giles Court, London.
- [24] Lasithiotakis M, Marsden B J, Marrow J T, Willets A. J Nucl Mater 2008; 381, 83–91.
- [25] Varhegyi G. J. Anal. Appl. Pyrol 2007; 79, 278–288.
- [26] Sorum L, Gronli M G, Hustad JE. Fuel 2001; 80, 1217-1227.
- [27] Joraid A A. Physica B. 2006; 390, 263-269.

- [28] Várhegyi G, Szabó P, Jakab E, Till F. J Anal Appl Pyrol 2001; 57, 203-222.
- [29] Hwang C L, Williams J L, Fan L T. Introduction to the generalized reduced gradient method. 1972 Institute for Systems Design and Optimization, Kansas State University in Manhattan. Report no. 39.
- [30] Lexa D, Dauke M. J Nucl Mater. 2009; 384, 236–244.
- [31] Kelly BT, Marsden BJ, Hall K, Martin DG, Harper A, Blanchard A. IAEA TEC DOC-1154, 2000.
- [32] Minshall P C, Wickam A J. IAEA TCM-Manchester99, 47-64.
- [33] Kitajima M, Asari E, Nakamura K G. J Nucl Mater 1994; 212-215, 139-142
- [34] Asari E, Kitajima M, Nakamura K G, Kawabe T. Phys Rev B 1993; 47, 147-156
- [35] Asari E, Kamioka I, Lewis WA, Kawabe T I, Nakamura K G, Kitajima M. Nucl Instrum Meth B. 1994; 91, 545-548
- [36] Li L, Reich S, Robertson J. Phys Rev B 2005; 72, 184109-184119
- [37] Tuinstra F, Koenig J L. J Chem Phys 1970; 53, 1126-1130
- [38] W.N. Reynolds, P.A. Thrower. Philos. Mag. 12, (1965) 573-593
- [39] R.H. Telling, C.P. Ewels, A.A. El-Barbary, M.I. Heggie, Nature Materials 2 (2003) 333-337
- [40] K.G. Nakamura, M. Kitajima, Phys. Rev. B 45 (1992) 5672.
- [41] K. Niwase, Int J Spec, 2012 (2012), 197609

[42] Urita K., Suenaga K, Sugai T, Shinohara H, Iijima S. Phys. Rev. Let .94, 155502
(2005)